Carbohydrate Polymers 94 (2013) 278–285

Contents lists available at SciVerse ScienceDirect

Carbohydrate Polymers

journal homepage: www.elsevier.com/locate/carbpol

Preparation of entangled nanocellulose fibers from APMP and its magnetic functional property as matrix

Wei Li, Xin Zhao, Shouxin Liu*

Key Laboratory of Bio-based Material Science and Technology of the Ministry of Education, Northeast Forestry University, Harbin 150040, China

ARTICLE INFO

Article history:
Received 23 November 2012
Received in revised form 7 January 2013
Accepted 18 January 2013
Available online 25 January 2013

Keywords:
Nanocellulose fiber
APMP
Ultrasonication
Aerogel
Magnetic

ABSTRACT

Nanocellulose fibers (NCFs) aerogels were prepared from poplar alkaline peroxide mechanical pulp (APMP) using physical ultrasonication method. As raw materials, the unique mechanical effects of APMP cause the fiber folding and loose during the pulping process, which was beneficial to further chemical purification and subsequent treatment for long and entangled NCFs. The obtained NCFs exhibited higher crystallinity (77.8%) compared with that of APMP (72.6%) together with diameters range from 20 to 90 nm and self-assembled to network. The primary thermal degradation of NCFs occurred at 331.5 °C. The prepared NCFs network aerogels acted as matrix which can prevent the growth and aggregation of ferromagnetic $CoFe_2O_4$ nanoparticles. The ratio of the $CoFe_2O_4$ of magnetic composites increased from 34 wt% to 75 wt%, and the magnetic properties were all increased with increasing the reaction concentration of $FeSO_4/CoCl_2$ salt.

1. Introduction

Cellulose is an abundant and naturally occurring polymer that can be obtained from many sources. Nano-sized single-crystal cellulose, which is commonly referred to as nanocrystalline cellulose, nanowhiskers or nanofibers, can be obtained from various sources such as natural fibers and sea animals (Habibi, Lucia, & Rojas, 2010). Nanocellulose fibers (NCFs) were an ideal candidate for medical, optical materials and reinforced composites due to its advantages of abundance, renewability and biodegradability, and excellent mechanical properties (Bhatnagar & Sain, 2005; Fleming, Gray, & Matthews, 2001; Ruiz, Cavaille, Dufresne, Graillat, & Gerard, 2001; Wegner & Jones, 2006; Zhang, Zhang, Lu, & Deng, 2012). Different approaches have been applied to the preparation of NCFs. Currently, acid hydrolysis methods are widely used for the removal of amorphous cellulose (Habibi et al., 2010). However, the use of acid has a number of important drawbacks, such as potential degradation of the cellulose, corrosivity, and environmental incompatibility. In addition, it significantly decreases the thermal stability of NCFs.

The isolation of NCFs from cellulose fibers using a simple, low cost and environment-friendly method is a great challenge (Wang & Cheng, 2009). Several mechanical processes have been used to extract NCFs from cellulosic materials. These methods include treatments, such as pulping beating (Iwamoto, Nakagaito, Yano, & Nogi, 2005; Nakagaito & Yano, 2004), high pressure homogenizing (Bruce, Hobson, Farrent, & Hepworth, 2005; Leitner, Hinterstoisser, Wastyn, Keches, & Gindl, 2007) and cryocrushing (Alemdar & Sain, 2008; Wang & Sain, 2007). Recently, the ultrasonic technique has been employed to isolate NCFs (Chen et al., 2011; Cheng, Wang, & Han, 2010). Among all NCFs preparation routes, ultrasonication seems to be a method well suited for isolating NCFs with relatively high lengths network (Cheng, Wang, Rials, & Lee, 2007; Cheng, Wang, & Rials, 2009; Tischer, Sierakowski, Westfahl, & Tischer, 2010). Ultrasonication is the application of sound energy to physical and chemical systems. The violent collapse induces microjets and shock waves on the surface of the purified cellulose fibers, causing erosion which leads to a split along the axial direction. The sonification impact can break the relatively weak interfaces between the microfibers bonded mainly by nonbonding interactions such as Van der Waals forces (Filson & Dawson-Andoh, 2009; Suslick, Choe, Cichowlas, & Grinstaff, 1991; Zhao, Feng, & Gao, 2007). The preparation of individual NCFs were investigated from wood using high-intensity ultrasonication combined with chemical pretreatments (Chen et al., 2011). The high-intensity ultrasonication was used in a batch process to isolate fibers from several cellulose sources. Using this process a mixture of microscale and nanoscale fibers was obtained (Cheng et al., 2010). Compared with above-mentioned materials, alkaline peroxide mechanical pulp, a relatively new process called the alkaline peroxide mechanical pulping (APMP) process reportedly produces pulp approaching the quality of chemical pulp while having yield and environmental impact approaching that of mechanical pulps. Meanwhile, it also had a relative high crystallinity (Yang, Lucia, Chen, Cao, & Liu, 2011).

* Corresponding author. Tel.: +86 451 82191204; fax: +86 451 82191204.
E-mail address: liushouxin@126.com (S. Liu).

0144-8617/$ – see front matter © 2013 Elsevier Ltd. All rights reserved.
http://dx.doi.org/10.1016/j.carbpol.2013.01.052

NCFs are excellent polymeric materials to improve the dispersion of nanoparticles. Nowadays, polymer–nanoparticle composites are attractive in applications requiring multifunctional characteristics, and their mechanical, optical and catalytic properties, among others, have been extensively explored (Balazs, Emrick, & Russell, 2006; Lin et al., 2005; Mackay et al., 2006; Warren et al., 2008). Above all, there is an increasing interest in magnetic ferrite nanoparticles because of their broad applications in several technological fields including permanent magnets, magnetic fluids, magnetic drug delivery, microwave devices, and high density information storage (Chinnasamy et al., 2003; Kitamoto, Kantake, Shirasaki, Abe, & Naoe, 1999). However, the high nanoparticle content may bring the problems of aggregation (Prozorov, Prozorov, & Gedanken, 1998). The challenge there is how to reduce nanoparticle aggregation and control the nanoparticles size at high concentrations, while other properties of the nanomaterials were not affected.

In our previous work, rod-like NCFs were prepared from MCC using high intensity ultrasonication without any additional chemical treatments and the ultrasonic mechanism was elaborate in depth in the preparation process (Li, Yue, & Liu, 2012). In the present work, APMP as starting material, high intensity ultrasonication was used to prepare long and entangled NCFs with uniform diameters. The chemical composition, morphology, crystalline structure, and thermal behavior of the NCFs and their intermediate products were characterized, respectively. Meanwhile, a magnetic composite was prepared using NCFs as matrix and the dispersion of magnetic particles was investigated.

2. Experiments

2.1. Preparation of NCFs

APMP with brightness of 82% ISO was used, which was obtained from poplar wood chips and kindly supplied by a pulp factory in Jilin Province of China. 2 g APMP was mixed into an acidified $NaClO_2$ solution at 75 °C for 1 h to remove lignin content; this process was repeated twice times, and the obtained holocellulose fibers (Ho-CFs) were further treated with 4 wt% NaOH at 80 °C for 2 h to remove hemicelluloses and residual lignin, the residues was filtered and rinsed with distilled water until pH = 7, the obtained solid product was alkali-treated cellulose fibers (Al-CFs). After then, the prepared Al-CFs was soaked in distilled water at approximately 0.2% (w/w) solid content. 150 mL Al-CFs solution was placed in an ultrasonic generator (JY98-IIID, Ningbo Scientz Biotechnology Co., Ltd., China) 20–25 kHz in frequency and equipped with a cylindrical titanium alloy probe tip 2.5 cm in diameter. The ultrasonication was conducted in an ice/water bath for 15 min at an output power of 900 W, resulting in a suspension of nanocellulose fibers (NCFs). The resulting suspension was centrifuged to separate the large bundles from the NCFs, and then were freeze-dried and stored at 5 °C for further test.

2.2. Preparation of magnetic NCFs

The NCFs aerogel pieces (20 mg) were immersed in 200 mL of freshly prepared aqueous solutions of $FeSO_4$ and $CoCl_2$ with a molar ratio of [Fe]/[Co] = 2. In brief, the NCFs were swelled for 15 min to ensure that a homogeneous distribution was obtained inside the NCFs networks. Three different solutions with total concentrations of the $FeSO_4/CoCl_2$ salts ([Fe]/[Co] = 2) of 0.03 mol/L (note as C_1), 0.09 mol/L (note as C_2) and 0.15 mol/L (note as C_3) were used. The systems were heated to 90 °C for 3 h to promote further transformation of soluble initial iron/cobalt hydroxides to insoluble iron/cobalt oxyhydroxide complexes. The NCFs network was then transferred into 200 mL of a 1.32 mol/L NaOH solution with KNO_3 ($[Fe^{2+}]/[NO^{3-}] = 0.44$) at 90 °C for 8 h. The particle-modified NCFs network was then washed thoroughly. The particle functionalized networks were immersed in liquid nitrogen and freeze-dried to generate the ferromagnetic aerogel nanocomposites (Olsson et al., 2005, 2010; Salazar-Alvarez et al., 2007).

2.3. Chemical composition measurement

The chemical composition of APMP, Ho-CFs, Al-CFs and NCFs were measured in accordance with the standards of Technical Association of Pulp and Paper Industry (TAPPI). The holocellulose (cellulose + hemicelluloses) content was determined as described in TAPPI T19 m-54. The α-cellulose content of the fibers was then determined by further NaOH treatment of the fibers to remove the hemicelluloses. The difference between the values of holocellulose and α-cellulose gives the hemicelluloses content of the fibers. The klason lignin content of the samples was determined as described in TAPPI T222 om-06. Three samples of each material were tested, and the averaged values were obtained. Degree of polymerization (DP) of BSKP and prepared NCC was measured by the viscosity method described by Iwamoto, Nakagaito, and Yano (2007).

2.4. Characterizations

Microstructural analysis was performed using a scanning electron microscope (FEI QUANTA200) (FEI, Hillsboro, OR, USA). The sample surfaces were coated with a thin layer of gold using a BAL-TEC SCD 005 sputter coater (Leica, Wetzlar, Germany) to provide electrical conductivity. Fourier transform infrared spectroscopy (FTIR) was carried out using a Magana-IR560E.S.P (Nicolet, USA) spectrometer to identify functional groups. X-ray diffraction XRD measurements were performed on a D/max-r B X-ray diffractometer (Rigaku Corp., Tokyo, Japan) using Cu Kα radiation. The samples were scanned over a 2θ range varying from 10° to 80°. The crystallinity index of cellulose materials was calculated from the height of the 2 0 0 peak (I_{200}, $2\theta = 22.6°$) and the intensity minimum between the peaks at 2 0 0 and 1 1 0 (I_{am}, $2\theta = 18°$) using the Segal method ($C_I\ (\%) = (1 - I_{am}/I_{200}) \times 100$). I_{200} represents both a crystalline and amorphous material, and I_{am} represents an amorphous material. Thermogravimetric analysis (TGA) was performed using a TG209-F3-Tarsus (NETZSCH, Selb, Germany) instrument. Temperature programs for dynamic tests were run from 25 °C to 600 °C at a heating rate of 10 °C/min. The BET surface area (S_{BET}), total pore volume and pore size of the samples were obtained from N_2 adsorption–desorption isotherms at 77 K using an Automated Surface and Pore Size Analyzer (ASAP 2020, Micromeritics, USA). Both adsorption and desorption isotherms were measured and the surface area was determined from the adsorption curve by the Brunauer–Emmet–Teller (BET) method. The mesopore diameter distributions were determined from desorption isotherms by the Barret–Joyner–Halenda (BJH) method. The magnetic measurements were carried out on an instrument of National Institute of Metrology P.R. China (Lake Shore 7410 VSM) at room temperature using a maximum applied field of 20 kG.

3. Results and discussion

3.1. Preparation of magnetic nanocellulose fibers aerogel

The synthesis pathway of NCFs and magnetic nanocomposites is described in Fig. 1. In order to obtain the higher purity of cellulose fibers from APMP (step a, Fig. 1), the lignin and most of the hemicellulose were removed according to methods with $NaClO_2$ and NaOH solutions, respectively (step b). Fibrillation on the cellulose surface can be clearly observed after chemical pre-treatment

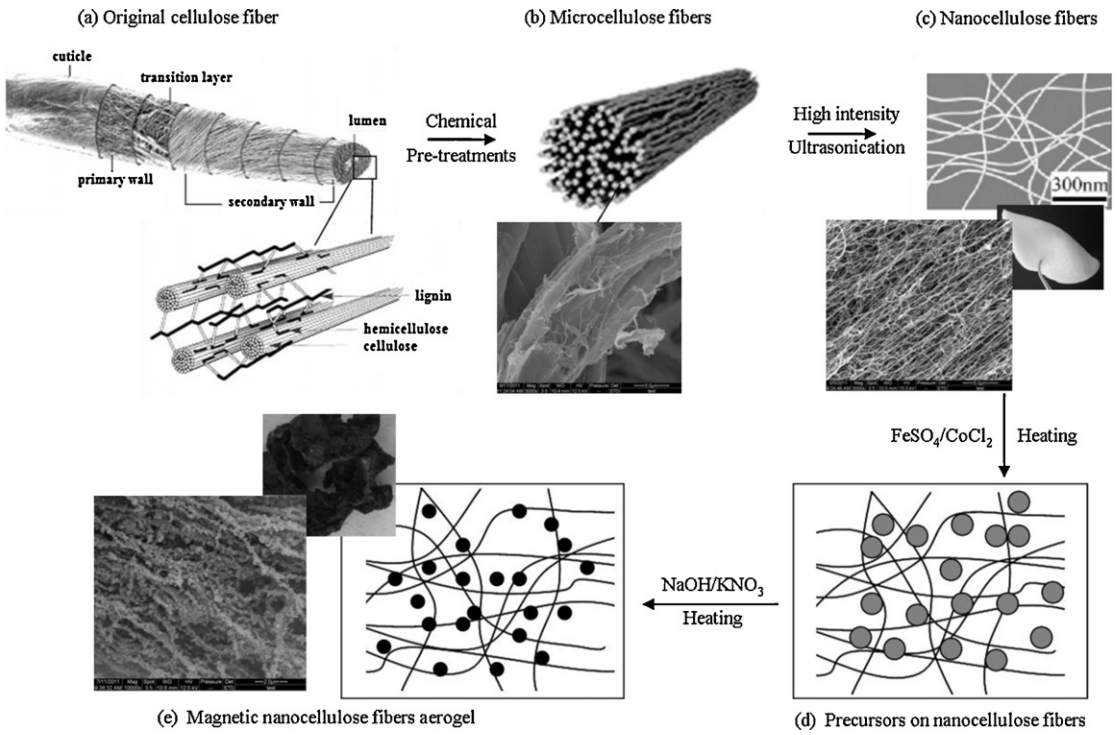

Fig. 1. Prepared procedures of magnetic nanocellulose fibers aerogel. (a) The structure of the original cellulose fiber; (b) the structure of the microcellulose fibers after chemical pre-treatments; (c) the structure of the nanocellulose fibers after high intensity ultrasonication treatment; (d) the magnetic precursors deposit on the surface of nanocellulose fibers; (e) the formation of magnetic nanocellulose fibers aerogel.

which indicated that the cohesion between the microcellulose fibers was reduced further. These changes were beneficial for the subsequent ultrasonic treatment to prepare the NCFs (step c). A freeze-dried porous NCFs aerogel matrix was immersed in an aqueous $FeSO_4/CoCl_2$ solution at ambient temperature (step d) before heating the system to thermally precipitate the metal hydroxides/oxides on the NCFs matrix. The precipitated precursors were transformed into ferrite crystal nanoparticles on immersion in $NaOH/KNO_3$ solution through heating (step e), resulting in magnetic aerogels. Micrographs of freeze-dried samples showed that the nanoparticles were located on the NCFs surfaces and dispersed well (step e, Fig. 1).

3.2. Cellulose fibers purification

The chemical composition changes of fibers with different pretreatment process are presented in Table 1. APMP contained the highest percentage of hemicelluloses (23.7%) and lignin (klason lignin 17.4% and acid–insoluble lignin 1.7%) and the lowest percentage of α-cellulose (55.9%). When the fibers were subjected to $NaClO_2$ treatment, the lignin content of the Ho-CFs decreased to 1.5%, whereas the α-cellulose and hemicelluloses content of the Ho-CFs increased to 68.7% and 29.8%, respectively. After NaOH treatment, the α-cellulose content of the Al-CFs increased to 88.7%, resulting in highly purified cellulose fibers. The cellulose fiber structure changed according to the removal of mainly components (Fig. 2). As raw cellulose fibers, the unique mechanical effects of APMP was due to its especial pulping process, caustic and hydrogen peroxide were used in the process to soften and brighten wood chips before refining in a disc refiner. After refining, the cohesion force of the fiber decreased and become looser and softer, the S1-layer was peeled into flakes (Fig. 2a) and the fibrillation extent of treated fiber enhance swelling and absorption capability which can more easily be permeated with $NaClO_2$ and NaOH solution, and also decreased the treatment time and amount of the chemical reagent in comparing with the previous report (Chen et al., 2011). However, there are no detailed changes of APMP surface that can be observed in Fig. 2b. The APMP surface exhibited some wrinkle and the local areas exhibited smooth relatively. The fiber structure was also maintained after $NaClO_2$ treatment removed most of the lignin. However, continuous web-like nanofibers are observed in the Ho-CFs due to the removal of the lignin (Fig. 2d). When NaOH treatment was performed to hydrolyze most hemicelluloses and residual lignin, fibrillation on the cellulose surface can be clearly observed (Fig. 2e and f). These changes were favorable to the subsequent high intensity ultrasonic treatment which can accumulate the ultrasonic stress for an efficient defibrillation process.

3.3. SEM analysis of NCFs

The structures of the aerogels consisting of NCFs are illustrated in Fig. 3. It is interesting to note that the long and entangled NCFs formed a network structure. When the dispersing aqueous medium was removed by freeze-drying, NCFs were assembled

Table 1
Chemical compositions and DP_n of APMP, Ho-CFs, Al-CFs and NCFs.

Material	α-Cellulose (%)	Hemicelluloses (%)	Klason lignin (%)	Acid–insoluble lignin (%)	DP_n
APMP	55.9 ± 1.4	23.7 ± 0.7	17.4 ± 1.2	1.7 ± 0.1	788 ± 12
HO-CFs	68.7 ± 1.5	29.8 ± 0.8	1.5 ± 0.1	–	765 ± 8
Al-CFs	88.7 ± 2.1	11.3 ± 0.4	–	–	743 ± 10
NCFs	90.4 ± 1.8	9.6 ± 0.2	–	–	657 ± 5

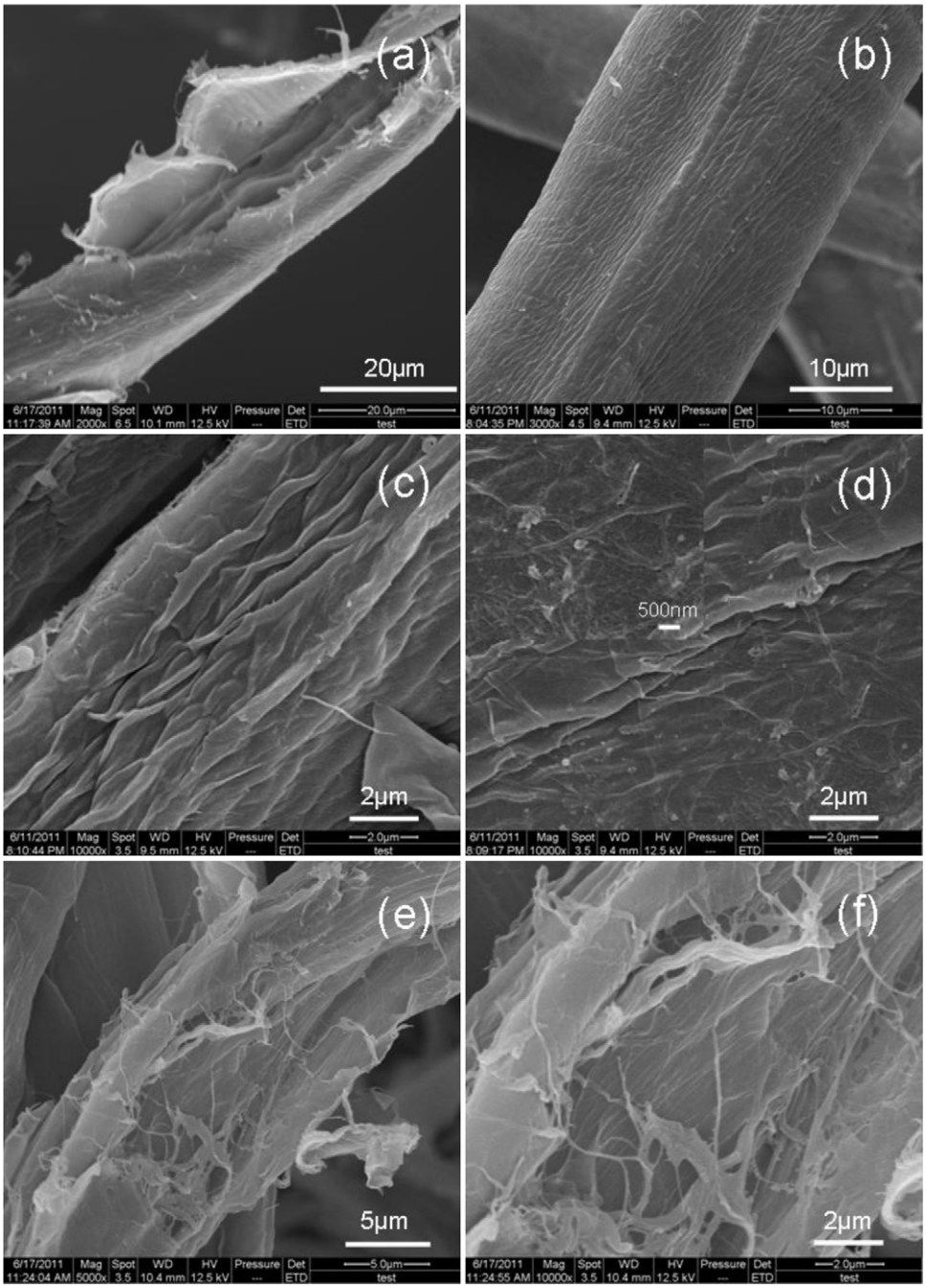

Fig. 2. SEM images of (a and b) the structure of the raw APMP; (c and d) the structure of fibers after acidified sodium chlorite treatment (Ho-CFs) (insert images shows the high magnification SEM graph of Ho-CFs), (e and f) the structure of the fibers after alkali-treated (Al-CFs).

approximately interlaced to each other. The low magnification SEM images (Fig. 3a and b) showed that the lengths of these individual NCFs were longer than 100 μm which was almost 500 times of the cellulose nanocrystals produced by acid hydrolysis methods (Beck-Candanedo, Roman, & Gray, 2005). About 70% NCFs were obtained with the diameters ranged from 20 to 90 nm (Fig. 3e). Moreover, as listed in Table 1, the DP_n of NCFs was 657, decreased only 16.6% comparing with that of APMP. This revealed that more long-chain polysaccharide of cellulose was maintained comparing with traditional acid hydrolysis method during chemical and ultrasonic process (Bondeson, Mathew, & Oksman, 2006). It was generally known that the scission of cellulose polymers bond as a result of solvodynamic shear was created by ultrasonic cavitation, which involves the nucleation, growth, and collapse of microbubbles in solution (Caruso et al., 2009). Certain sizes of ultrasonic cavitation bubbles in the liquid medium may suddenly be collapsed, creating powerful shock waves, and generating a large amount of mechanical and thermal energy in the liquid. A liquid jet propagates toward the cellulose surface at a velocity of several hundred meters per second, and makes violent contact with the cellulose surface resulting in the morphology changes of cellulose. Fig. 2f and g shows a NCFs sheet that is light and flexible. Based on the adsorption isotherms and the BET equation, surface areas were calculated. The Barrett–Joyner–Halenda method was used to analyze and characterize the pore structures of the NCFs. The S_{BET} and average pore width of NCFs sheet were 23.4 $m^2 g^{-1}$ and 13.4 nm, respectively. Such a porous sheet consisting of long and entangled NCFs, are expected to be used in various applied fields, such as reinforcement

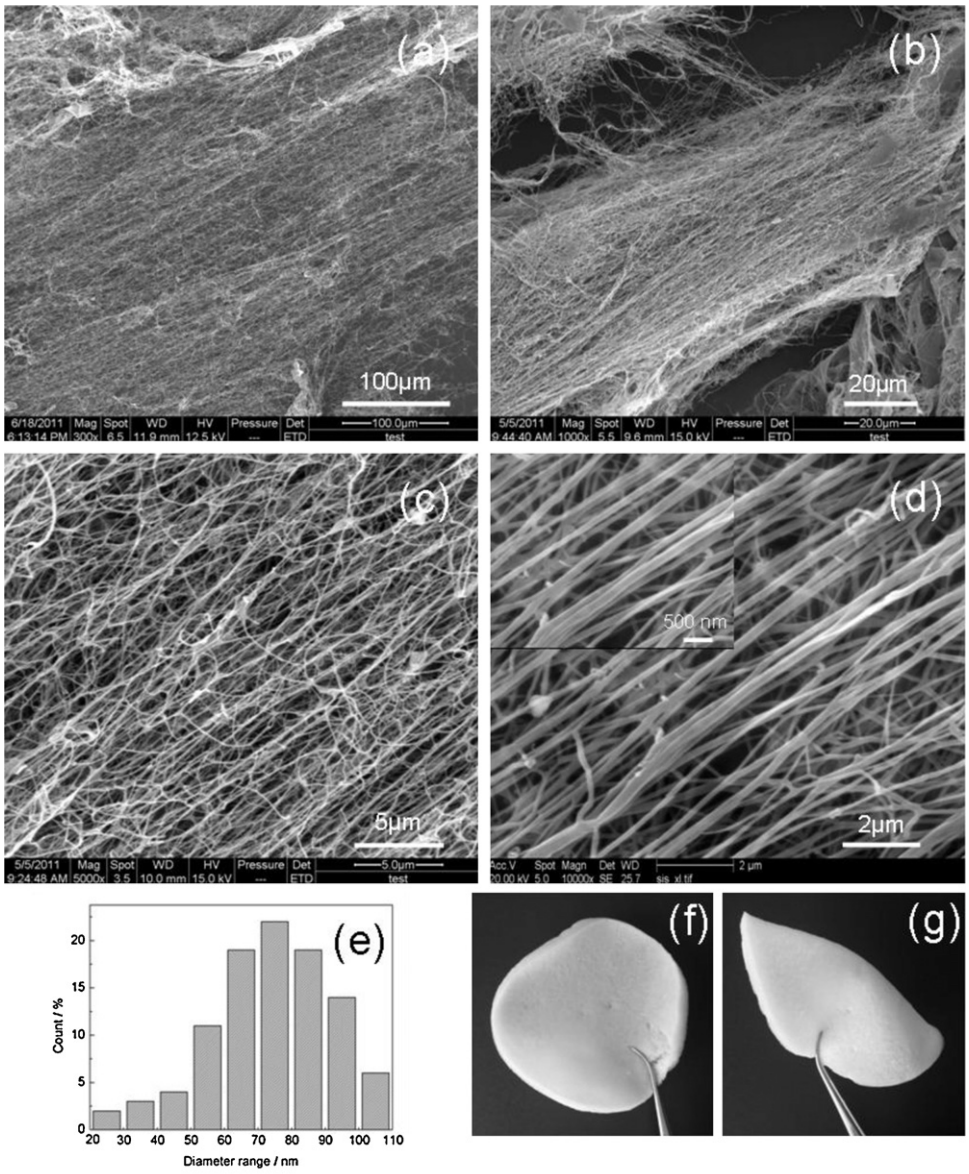

Fig. 3. SEM images of (a–d) of NCFs; (e) diameter distribution of NCFs and (f and g) photographs of NCFs sheet.

nanocomposites, advanced functional material, fiter membrane; and opened new possibilities for templating inorganic matter for various functionalities.

3.4. FT-IR and XRD analysis of APMP, Ho-CFs, Al-CFs and NCFs

FT-IR spectra of APMP, Ho-CFs, Al-CFs and NCFs are shown in Fig. 4a. The 1506 and 1459 cm^{-1} peaks of APMP represent the C=C stretching vibration in aromatic ring vibration and C—H deformation vibration of lignin, respectively (Sain & Panthapulakkal, 2006; Sun, Tomkinson, Wang, & Xiao, 2000). The intensity of these peaks almost disappeared for Ho-CFs, which is attributed to the removal of most of lignin. The peaks at 1733 cm^{-1} of Ho-CFs represent either the acetyl and uronic ester groups or the ester linkage of carboxylic group of the ferulic and p-coumeric acids of hemicelluloses (Alemdar & Sain, 2008; Chen et al., 2011). These were further confirmed according to the result in Table 1. After ultrasonic treatment, the spectrum of the NCFs was almost similar to that of the Al-CFs. This fact indicated that a larger amount of hemicelluloses and lignin were removed during the treatment of $NaClO_2$ and NaOH; and the original molecular structure of cellulose was maintained even after these components removal and ultrasonic treatments.

Fig. 4b is the X-ray diffraction profiles and the crystallinity of APMP, Ho-CFs, Al-CFs and NCFs. All samples had diffraction peaks at $2\theta = 16.5^{\circ}$ and 22.5° and were believed to represent the typical cellulose I pattern (Nishiyama, Sugiyama, Chanzy, & Langan, 2003). The crystallinity of APMP was 72.6%. After $NaClO_2$ treatment, the crystallinity of Ho-CFs increased to 74.7% owing to the removal of lignin. The crystallinity of Al-CFs increased to 75.6% because of the hemicelluloses removal which exist in the amorphous regions. After ultrasonic treatment, the crystallinity of NCFs increased to 77.8%. From the XRD profiles of NCFs, it can be observed that the intensity of amorphous and crystalline areas were all decreased. This means that it can remove both amorphous and crystalline cellulose. The increase in crystallinity may due to slow decline in the proportion of crystalline areas (Li et al., 2012). The ultrasonic activation effect in heterogeneous systems is primarily the consequence of cavitation. In the CFs–water system, both the crystalline and amorphous regions were subjected intense collisions (Cintas & Luche, 1999). It can be concluded that on the CFs surface, the intense physical stresses cause hydrogen bond breakage between

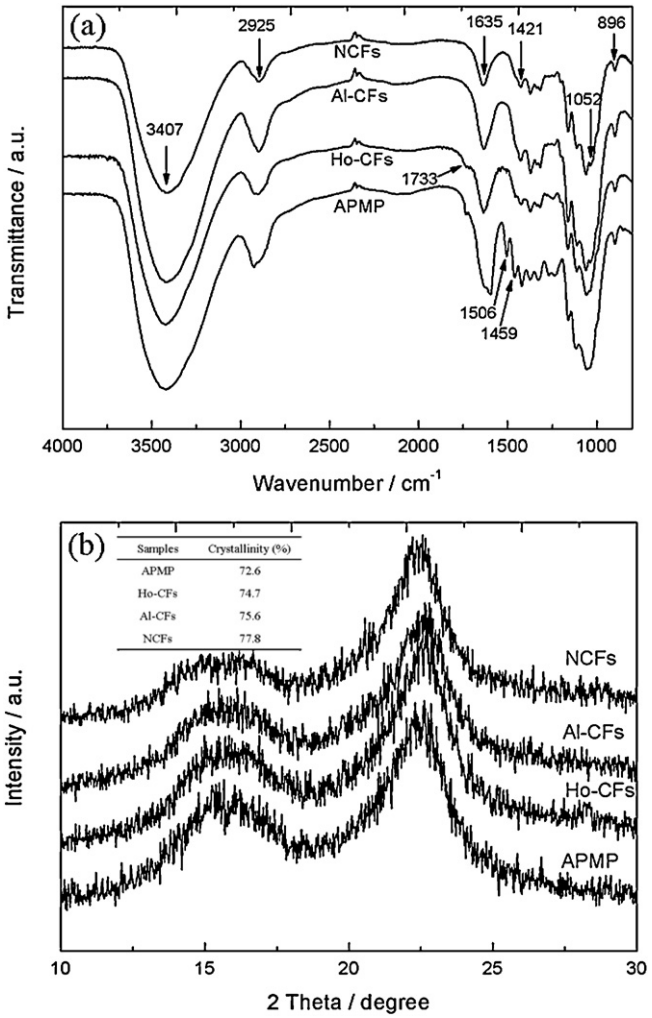

Fig. 4. FT-IR spectra (a) X-ray diffraction patterns (b) of APMP, Ho-CFs, Al-CFs, and NCFs.

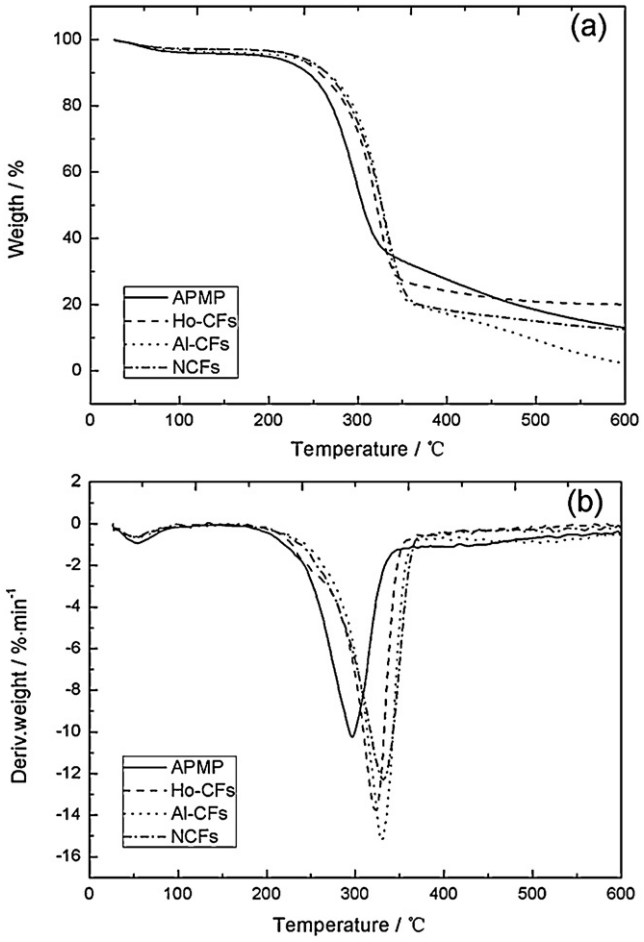

Fig. 5. TGA (a) and DTG (b) curves for APMP, Ho-CFs, Al-CFs and NCFs.

the microfibers of CFs and then defibrillated to NCFs. The high crystallinity of NCFs could be more effective in providing better strength for composite materials (Sakurada, Nukushina, & Ito, 1962). The ratio of such amorphous regions to the crystalline regions is a critical parameter in the design of preparation methods for NCFs (Hamad, 2006). The isolation of perfect crystals requires the consideration of many factors, such as the significant crystallinity, yield and economic efficiency. Therefore, we concluded that a 15 min ultrasonication (900 W) was a high-efficiency technology for preparing NCFs in comparing with the previous reports (Chen et al., 2011).

3.5. TG and DTG analysis

Fig. 5 shows thermogravimetric curves of APMP, Ho-CFs, Al-CFs and NCFs. All of them showed a slight weight loss at low temperature (<150 °C), which corresponds to the evaporation of absorbed water. The primary degradation of APMP corresponds to the pyrolysis of cellulose occurred at 265.5 °C, and the dominant peak was observed at 296.4 °C (Fig. 5b). Due to the removal of lignin, the initial degradation and the main degradation peak of Ho-CFs increased

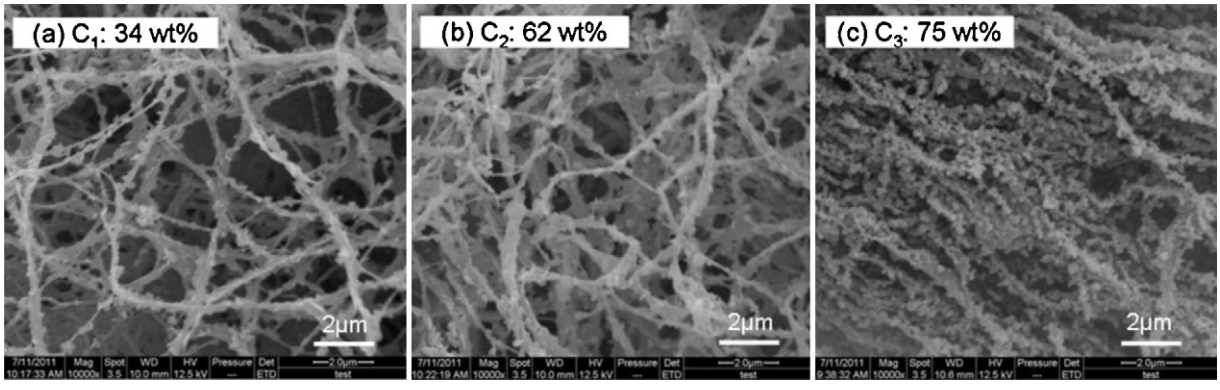

Fig. 6. SEM images of magnetic NCFs (a) C_1, (b) C_2 and (c) C_3.

Table 2
Crystallite size and magnetic properties of the magnetic NCFs at different reaction concentration.

Sample	Average crystallite sizes (nm)	Coercivity (Hc) (Oe)	Magnetization (Ms) (emu/g)	Retentivity (Mr/Ms)
C_1	31.1	478.51	19.211	0.30
C_2	32.4	733.63	21.466	0.41
C_3	32.8	862.63	50.024	0.48

to 294.9 °C and 322.6 °C, respectively. After most parts of the hemicelluloses were hydrolyzed by NaOH treatment, the degradation of Al-CFs increased to 303.1 °C. For NCFs, the degradation started at 296.4 °C. The initial pyrolysis temperature shifted to a lower temperature, due to the increased hydroxyl groups (Glasser, Taib, Jain, & Kander, 1999).

3.6. SEM analysis of magnetic NCFs aerogels

The magnetic nanoparticles fraction can be controlled by adjusting the total concentration of the $FeSO_4/CoCl_2$ salts using NCFs as matrix. SEM images of magnetic NCFs prepared by different magnetic nanoparticle of $CoFe_2O_4$ content of 34, 62 and 75 wt%, respectively are shown in Fig. 6. $CoFe_2O_4$ particles were combined closely together with the NCFs after rinsing. It indicated that the metal oleation/oxolation was affected in the presence of the NCFs matrix (Jolivet, Chanéac, & Tronc, 2004; Salazar-Alvarez et al., 2007). The dispersity of the magnetic particles was excellent with increasing of the concentration of the $FeSO_4/CoCl_2$ salts. Even the content of $CoFe_2O_4$ was up to 75%, the nanoparticles still showed an excellent dispersion (Fig. 6c). A mechanism of formation of the nanoparticles is presented (Fig. 1). First, a nano-scale or micro-scale reactor that was formed by bonding between the hydroxyl groups of NCFs long-chain during the freeze-dried process which can inhibit the growth and aggregation of the magnetic precursors. And also, the reactions simultaneously proceeded within the NCFs inside network reactor as well as within the absorbed metal hydroxo/oxo cation layer on the NCFs. Second, the hydroxo/oxo cation complexes may also adsorb on the NCFs surfaces via proton exchange reactions with the cellulose hydroxyl groups (Jolivet et al., 2004; Olsson et al., 2005, 2010; Salazar-Alvarez et al., 2007).

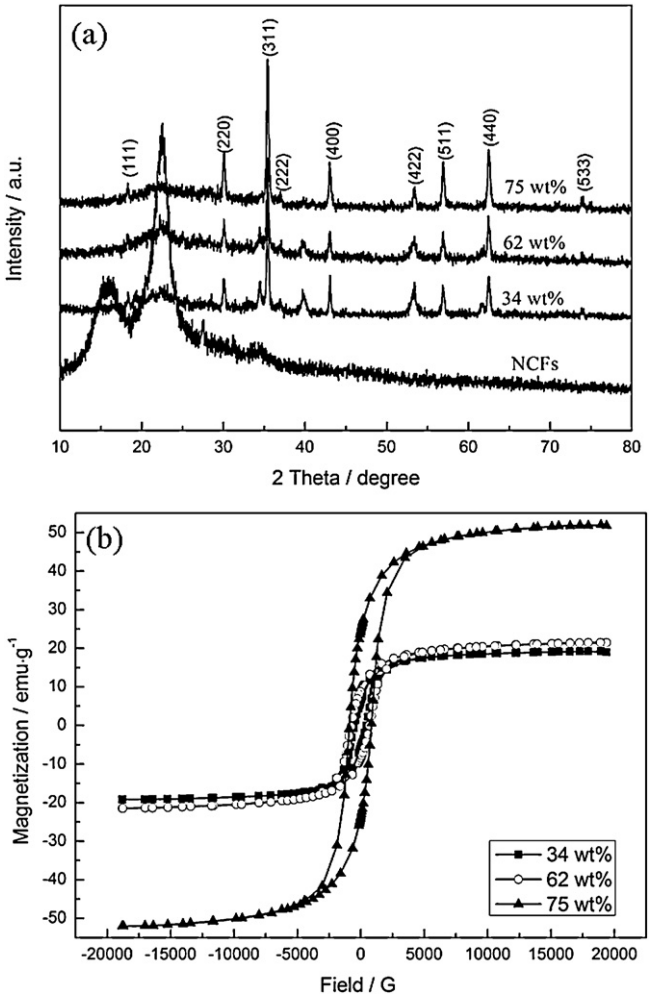

Fig. 7. (a) X-ray diffraction patterns for NCFs and magnetic NCFs and (b) magnetic properties of nanocomposites.

3.7. XRD and magnetic properties analysis of magnetic NCFs aerogels

The XRD patterns of magnetic NCFs (Fig. 7a) confirmed the presence of spinel type lattice of $CoFe_2O_4$ (JCPSD nos. 22-1086). The average crystallite sizes of $CoFe_2O_4$ particles were determined from the full-width at half maximum of the (3 1 1) peak using the well-known Scherrer equation (Jiang, Rühle, & Lavernia, 1999; Qu et al., 2006) and results are presented in Table 2. It is shown that the average crystallite size increase slightly with increasing of the metal salt concentration. This indicated that lower reaction concentrations were suitable for the control the $CoFe_2O_4$ crystals grow.

Magnetic properties of the prepared magnetic NCFs were measured at room temperature with VSM. The hysteresis loops are shown in Fig. 7b. The coercivity, magnetization and the remanence ration were all increased with increasing of the reaction concentration. The nanocomposites exhibit coercivities (Hc = 478.51, 733.63 and 862.63 Oe for C_1, C_2 and C_3, respectively) and saturation magnetization per ferrite volume (Ms = 19.211, 21.466 and 50.024 emu/g for C_1, C_2 and C_3, respectively). When the concentration was 0.09 mol/L (C_2), Hc increased from 478.51(C_1) to 733.63 G and Ms changed slightly. When the concentration was 0.15 mol/L (C_3), Ms reached to 50.024 from 21.466 (C_2) and the Hc only changed from 733.63 G to 862.63 G. This indicated that a critical reactive concentration between the 0.09 mol/L and 0.15 mol/L is existed.

4. Conclusions

We have demonstrated a facile approach to constructing a kind of longer and entangled network NCFs with diameter of 20–90 nm from poplar APMP by using high intensity ultrasonication. The NCFs was mainly cellulose because the cellulose I crystal structure was maintained, with the removal of the lignin and parts of hemicelluloses during the chemical process. The obtained NCFs exhibited higher crystallinity (77.8%) compared with that of APMP (72.6%). The main thermal degradation temperature of the NCFs (331.5 °C) was higher than that of APMP (296.4 °C) duo to removal of the lignin and parts of the hemicelluloses. Also, magnetic $CoFe_2O_4$ nanoparticles were precipitated on a NCFs matrix in order to improve the dispersity of the nanoparticles. The ratio of the $CoFe_2O_4$ of magnetic composites, coercivity, magnetization and remanence ratio increased with the increasing of the concentration of the $FeSO_4/CoCl_2$ salt. Because the concepts of the procedure were relatively simple and NCFs was sustainable and

renewable from different plants, the suggested route in preparing NCFs and nanocomposites were suitable for industrial-scale production and also can be used to prepare many other kinds of nanoparticles.

Acknowledgements

This project was supported financially by the Research Fund for the Fundamental Research Funds for the Central Universities (DL11EB01), the National Natural Science Foundation of China (No. 31170545) and the Foundation of Excellent Doctoral Dissertation of NEFU (Grap09).

References

Alemdar, A., & Sain, M. (2008). Isolation and characterization of nanofibers from agricultural residues – Wheat straw and soy hulls. *Bioresource Technology*, *99*(6), 1664–1671.

Balazs, A. C., Emrick, T., & Russell, T. P. (2006). Nanoparticle polymer composites: Where two small worlds meet. *Science*, *314*, 1107–1110.

Beck-Candanedo, S., Roman, M., & Gray, D. G. (2005). Effect of reaction conditions on the properties and behavior of wood cellulose nanocrystal suspensions. *Biomacromolecules*, *6*, 1048–1054.

Bhatnagar, A., & Sain, M. J. (2005). Processing of cellulose nanofiber-reinforced composites. *Journal of Reinforced Plastics and Composites*, *24*(12), 1259–1268.

Bondeson, D., Mathew, A., & Oksman, K. (2006). Optimization of the isolation of nanocrystals from microcrystalline cellulose by acid hydrolysis. *Cellulose*, *13*, 171–180.

Bruce, D. M., Hobson, R. N., Farrent, J. W., & Hepworth, D. G. (2005). High performance composites from low-cost plant primary cell walls. *Composites Part A: Applied Science and Manufacturing*, *36*(11), 1486–1493.

Caruso, M. M., Davis, D. A., Shen, Q. L., Odom, S. A., Sottos, N. R., White, S. R., et al. (2009). Mechanically-induced chemical changes in polymeric materials. *Chemical Reviews*, *109*(11), 5755–5798.

Cheng, Q. Z., Wang, S. Q., & Han, Q. Y. (2010). Novel process for isolating fibrils from cellulose fibers by high-intensity ultrasonication. II. Fibril characterization. *Journal of Applied Polymer Science*, *115*, 2756–2762.

Cheng, Q. Z., Wang, S. Q., & Rials, T. G. (2009). Poly(vinyl alcohol) nanocomposites reinforced with cellulose fibrils isolated by high intensity ultrasonication. *Composites Part A: Applied Science and Manufacturing*, *40*(2), 218–224.

Cheng, Q. Z., Wang, S. Q., Rials, T., & Lee, S. (2007). Physical and mechanical properties of polyvinyl alcohol and polypropylene composite materials reinforced with fibril aggregates isolated from regenerated cellulose fibers. *Cellulose*, *14*(6), 593–602.

Chen, W. S., Yu, H. P., Liu, Y. X., Chen, P., Zhang, M. X., & Hai, Y. F. (2011). Individualization of cellulose nanofibers from wood using high-intensity ultrasonication combined with chemical pretreatments. *Carbohydrate Polymers*, *83*, 1804–1811.

Chinnasamy, C. N., Senoue, M., Jeyadevan, B., Perales-Perez, O., Shinoda, K., & Tohji, K. (2003). Synthesis of size-controlled cobalt ferrite particles with high coercivity and squareness ratio. *Journal of Colloid and Interface Science*, *263*, 80–83.

Cintas, P., & Luche, J. L. (1999). Green chemistry: The sonochemical approach. *Green Chemistry*, *1*, 115–125.

Filson, P. B., & Dawson-Andoh, B. E. (2009). Sono-chemical preparation of cellulose nanocrystals from lignocellulose derived materials. *Bioresource Technology*, *100*, 2259–2264.

Fleming, K., Gray, D. G., & Matthews, S. (2001). Cellulose crystallites. *Chemistry – A European Journal*, *7*(9), 1831–1835.

Glasser, W. G., Taib, R., Jain, R. K., & Kander, R. (1999). Fiber-reinforced cellulosic thermoplastic composites. *Journal of Applied Polymer Science*, *73*, 1329–1340.

Habibi, Y., Lucia, L. A., & Rojas, O. J. (2010). Cellulose nanocrystals: Chemistry, self-assembly, and applications. *Chemical Reviews*, *110*, 3479–3500.

Hamad, W. (2006). On the development and applications of cellulosic nanofibrillar and nanocrystalline materials. *Canadian Journal of Chemical Engineering*, *10*, 513–519.

Iwamoto, S., Nakagaito, A. N., & Yano, H. (2007). Nano-fibrillation of pulp fibers for the processing of transparent nanocomposites. *Applied Physics A: Materials Science and Processing*, *89*(2), 461–466.

Iwamoto, S., Nakagaito, A. N., Yano, H., & Nogi, M. (2005). Optically transparent composites reinforced with plant fiber-based nanofibers. *Applied Physics A: Materials Science and Processing*, *81*, 1109–1112.

Jiang, H. G., Rühle, M., & Lavernia, E. J. (1999). On the applicability of the X-ray diffraction line profile analysis in extraction grain size and microstrain in nanocrystalline materials. *Journal of Materials Research*, *14*, 549–559.

Jolivet, J. P., Chanéac, C., & Tronc, E. (2004). Iron oxide chemistry. From molecular clusters to extended solid networks. *Chemical Communications*, *5*, 481–487.

Kitamoto, Y., Kantake, S., Shirasaki, S., Abe, F., & Naoe, M. (1999). Coferrite films with excellent perpendicular magnetic anisotropy and high coercivity deposited at low temperature. *Journal of Applied Physics*, *85*, 4708–4710.

Leitner, J., Hinterstoisser, B., Wastyn, M., Keches, J., & Gindl, W. (2007). Sugar beet cellulose nanofibril-reinforced composites. *Cellulose*, *14*(5), 419–425.

Li, W., Yue, J. Q., & Liu, S. X. (2012). Preparation of nanocrystalline cellulose via ultrasound and its reinforcement capability for poly(vinyl alcohol) composites. *Ultrasonics Sonochemistry*, *19*, 479–485.

Lin, Y., Boker, A., He, J. B., Sill, K., Xiang, H. Q., Abetz, C., et al. (2005). Self-directed self-assembly of nanoparticle/copolymer mixtures. *Nature*, *434*, 55–59.

Mackay, M. E., Tuteja, A., Duxbury, P. M., Hawker, C. J., Horn, B. V., Guan, Z. B., et al. (2006). General strategies for nanoparticle dispersion. *Science*, *311*, 1740–1743.

Nakagaito, A. N., & Yano, H. (2004). The effect of morphological changes from pulp fiber towards nano-scale fibrillated cellulose on the mechanical properties of high strength plant fiber based composites. *Applied Physics A: Materials Science and Processing*, *78*(4), 547–552.

Nishiyama, Y., Sugiyama, J., Chanzy, H., & Langan, P. (2003). Crystal structure and hydrogen bonding system in cellulose Iα from synchrotron X-ray and neutron fiber diffraction. *Journal of the American Chemical Society*, *125*(47), 14300–14306.

Olsson, R. T., Azizi Samir, M. A. S., Salazar-Alvarez, G. S., Belova, L., Strom, V., Berglund, L. A., et al. (2010). Making flexible magnetic aerogels and stiff magnetic nanopaper using cellulose nanofibrils as templates. *Nature Nanotechnology*, *5*, 584–588.

Olsson, R. T., Salazar-Alvarez, G., Hedenqvist, M. S., Gedde, U. W., Lindberg, F., & Savage, S. J. (2005). Controlled synthesis of near-stoichiometric cobalt ferrite nanoparticles. *Chemistry of Materials*, *17*, 5109–5118.

Prozorov, T., Prozorov, R., & Gedanken, A. (1998). Does the self-assembled coating of magnetic nanoparticles cover individual particles or agglomerates. *Advanced Materials*, *10*, 1529–1532.

Qu, Y. Q., Yang, H. B., Yang, N., Fan, Y. Z., Zhu, H. Y., & Zou, G. T. (2006). The effect of reaction temperature on the particle size, structure and magnetic properties of coprecipitated $CoFe_2O_4$ nanoparticles. *Materials Letters*, *60*, 3548–3552.

Ruiz, M. M., Cavaille, J. Y., Dufresne, A., Graillat, C., & Gerard, J. F. (2001). New waterborne epoxy coatings based on cellulose nanofillers. *Macromolecular Symposium*, *169*, 211–222.

Sain, M., & Panthapulakkal, S. (2006). Bioprocess preparation of wheat straw fibers and their characterization. *Industrial Crops and Products*, *23*(1), 1–8.

Sakurada, I., Nukushina, Y., & Ito, T. (1962). Experimental determination of the elastic modulus of crystalline regions in oriented polymers. *Journal of Polymer Science*, *57*(165), 651–660.

Salazar-Alvarez, G., Olsson, R. T., Sort, J., Macedo, W. A. A., Ardisson, J. D., Baró, M. D., et al. (2007). Enhanced coercivity in Co-rich near-stoichiometric $Co_xFe_{3-x}O_{4+\sigma}$ nanoparticles prepared in large batches. *Chemistry of Materials*, *19*, 4957–4963.

Sun, R. C., Tomkinson, J., Wang, Y. X., & Xiao, B. (2000). Physico-chemical and structural characterization of hemicelluloses from wheat straw by alkaline peroxide extraction. *Polymer*, *41*(7), 2647–2656.

Suslick, K. S., Choe, S. B., Cichowlas, A. A., & Grinstaff, M. W. (1991). Sonochemical synthesis of amorphous iron. *Nature*, *353*, 414–416.

Tischer, P. C. S. F., Sierakowski, M. R., Westfahl, H., & Tischer, C. A. (2010). Nanostructural reorganization of bacterial cellulose by ultrasonic treatment. *Biomacromolecules*, *11*(5), 1217–1224.

Wang, B., & Sain, M. (2007). Dispersion of soybean stock-based nanofiber in a plastic matrix. *Polymer International*, *56*(4), 538–546.

Wang, S. Q., & Cheng, Q. Z. (2009). A novel process to isolate fibrils from cellulose fibers by high-intensity ultrasonication. Part 1: Process optimization. *Journal of Applied Polymer Science*, *113*, 1270–1275.

Warren, S. C., Messina, L. C., Slaughter, L. S., Kamperman, M., Zhou, Q., Gruner, S. M., et al. (2008). Ordered mesoporous materials from metal nanoparticle-block copolymer self-assembly. *Science*, *320*, 174–1752.

Wegner, T. H., & Jones, P. E. (2006). Advancing cellulose-based nanotechnology. *Cellulose*, *13*, 115–118.

Yang, G. H., Lucia, L. A., Chen, J. C., Cao, X. D., & Liu, Y. (2011). Effects of enzyme pretreatment on the beatability of fast-grawing poplar APMP pulp. *Bioresources*, *6*(3), 2568–2580.

Zhang, W., Zhang, Y. A., Lu, C. H., & Deng, Y. L. (2012). Aerogels from crosslinked cellulose nano/micro-fibrils and their fast shape recovery property in water. *Journal of Materials Chemistry*, *22*, 11642–11650.

Zhao, H., Feng, X., & Gao, H. (2007). Ultrasonic technique for extracting nanofibers from nature materials. *Applied Physics Letters*, *90*, 073112.